iScience

CellPress
OPEN ACCESS

Article

Human adipose ECM alleviates radiation-induced skin fibrosis via endothelial cell-mediated M2 macrophage polarization

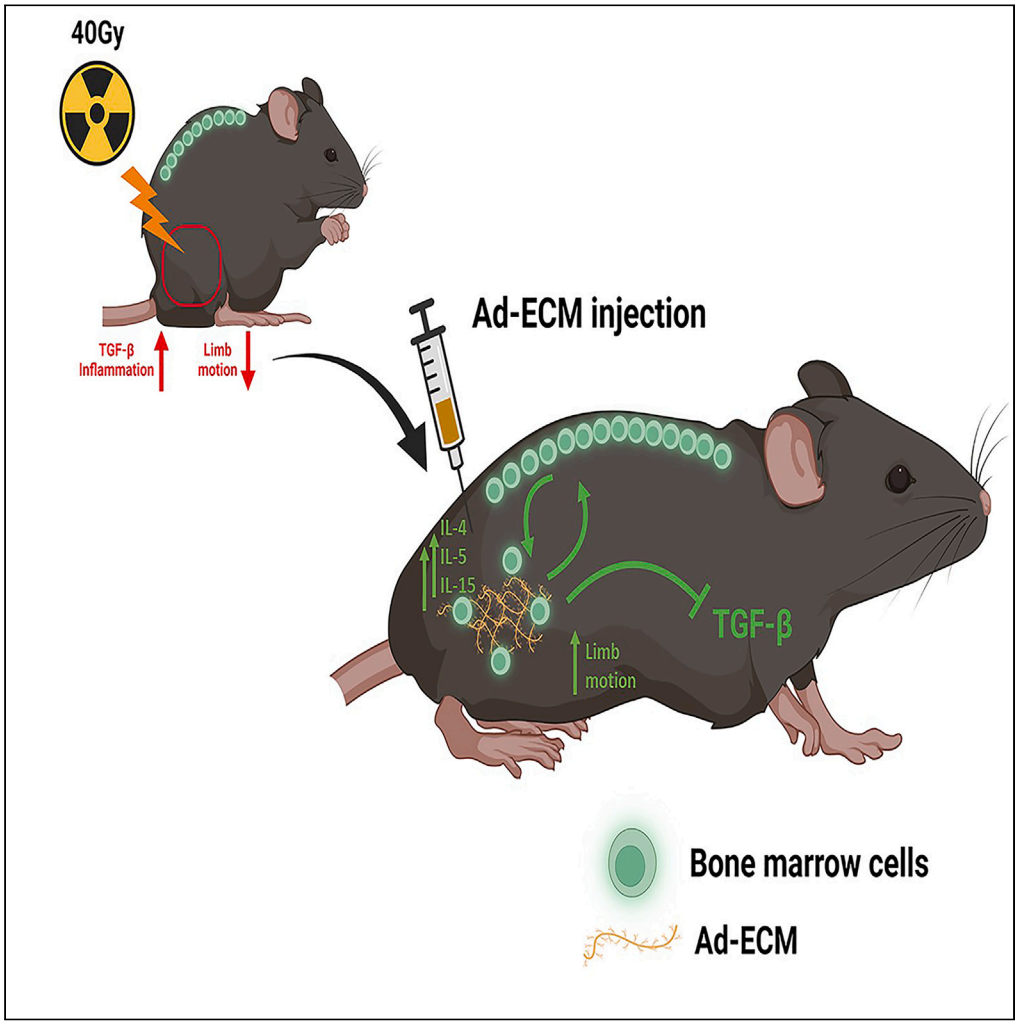

Somaiah Chinnapaka, Katherine S. Yang, Yusuf Surucu, ..., Joel S. Greenberger, J. Peter Rubin, Asim Ejaz

ejaza@upmc.edu

Highlights

Ad-ECM can effectively mitigate RISF

M2 macrophage polarization plays a crucial role in mitigation

Ad-ECM offers prophylactic mitigation potential to RISF

Chinnapaka et al., iScience 26, 107660
September 15, 2023
https://doi.org/10.1016/j.isci.2023.107660

iScience

CellPress
OPEN ACCESS

Article

Human adipose ECM alleviates radiation-induced skin fibrosis via endothelial cell-mediated M2 macrophage polarization

Somaiah Chinnapaka,[1,3] Katherine S. Yang,[1,3] Yusuf Surucu,[1,3] Fuat B. Bengur,[1] José A. Arellano,[1] Zayaan Tirmizi,[1] Hamid Malekzadeh,[1] Michael W. Epperly,[2] Wen Hou,[2] Joel S. Greenberger,[2] J. Peter Rubin,[1] and Asim Ejaz[1,4,*]

SUMMARY

Radiation therapy can lead to late radiation-induced skin fibrosis (RISF), causing movement restriction, pain, and organ dysfunction. This study evaluated adipose-derived extracellular matrix (Ad-ECM) as a mitigator of RISF. Female C57BL/6J mice that were irradiated developed fibrosis, which was mitigated by a single local Ad-ECM injection, improving limb movement and reducing epithelium thickness and collagen deposition. Ad-ECM treatment resulted in decreased expression of pro-inflammatory and fibrotic genes, and upregulation of anti-inflammatory cytokines, promoting M2 macrophage polarization. Co-culture of irradiated human fibroblasts with Ad-ECM down-modulated fibrotic gene expression and enhanced bone marrow cell migration. Ad-ECM treatment also increased interleukin (IL)-4, IL-5, and IL-15 expression in endothelial cells, stimulating M2 macrophage polarization and alleviating RISF. Prophylactic use of Ad-ECM showed effectiveness in mitigation. This study suggests Ad-ECM's potential in treating chronic-stage fibrosis.

INTRODUCTION

Radiation therapy is the cornerstone of modern cancer therapy, and almost 50% of cancer patients can benefit from radiotherapy in the management of their disease.[1] Controlled radiation dose can cause DNA damage in healthy cells. Although modern technological advancements in therapy application result in minimal bystander normal tissue damage, it is still one of the major side effects.[2] Skin is the first line of defense protecting the body from external hazards. Ionizing irradiation-induced tissue damage in skin and muscle is a recognized late side effect of radiation therapy. In addition, exposure to radiation generated as a result of accidents, war, or terrorism affects the skin. Late effects can be progressive and severe. Radiation-induced skin fibrosis (RISF) results in progressive functional and anatomic impairment[3] including decreased tissue elasticity, limited mobility, atrophy, telangiectasias, xerosis, poor wound healing, alopecia, fibrosis of follicles and sebaceous glands, pigmentation changes, and necrosis.[4]

RISF results from a complex process that involves the dysregulated function of several cellular and non-cellular factors after radiation injury, causing excessive production and deposition of extracellular matrix (ECM) at the radiation injury site.[5] Radiation exposure results in initial damage to epithelial and endothelial cells lining the vasculature resulting in hypocellularity and hypoxia characterized by upregulated GM-CSF and macrophage colony stimulating factor (M-CSF) levels.[6] Myofibroblasts, the major player in the process of fibrogenesis, are derived from tissue-resident or migratory fibroblasts and are associated with tissue repair and fibrosis.[7,8] After normal wound healing, myofibroblasts undergo apoptosis. However, upon radiation injury, the perpetual cycle of inflammatory signals drives the differentiation of fibroblasts to myofibroblasts which are then responsible for the excessive deposition of the ECM.[9] The pro-fibrotic role of transforming growth factor (TGF)-β1 is supported by the observation that exogenous injection of TGF-β1 or genetic manipulation to overexpress TGF-β1 in mice results in the development of fibrosis.[10] Triggering events, such as wound healing or ionizing radiation exposure, induce activation of TGF-β1 within hours.[11,12] TGF-β1 regulates ECM remodeling by balancing its synthesis and degradation. Irradiation disrupts this balance through a simultaneous upregulation of genes responsible for ECM synthesis and downregulation of the matrix-degrading proteases.[13]

Autologous fat grafting demonstrates promising preclinical and clinical manifestations in post-radiation damage.[14] Rigotti et al. reported an improvement in fibrosis and Late Effects Normal Tissue Task Force (LENT)-Subjective, Objective, Management, Analytic (SOMA) score attributed to enhanced vascularization and were able to induce healing in a refractory irradiated chest wound.[15] Fat grafting in irradiated

[1]Department of Plastic Surgery, University of Pittsburgh, Pittsburgh, PA, USA
[2]Department of Radiation Oncology, University of Pittsburgh Cancer Institute, Pittsburgh, PA, USA
[3]These authors contributed equally
[4]Lead contact
*Correspondence: ejaza@upmc.edu
https://doi.org/10.1016/j.isci.2023.107660

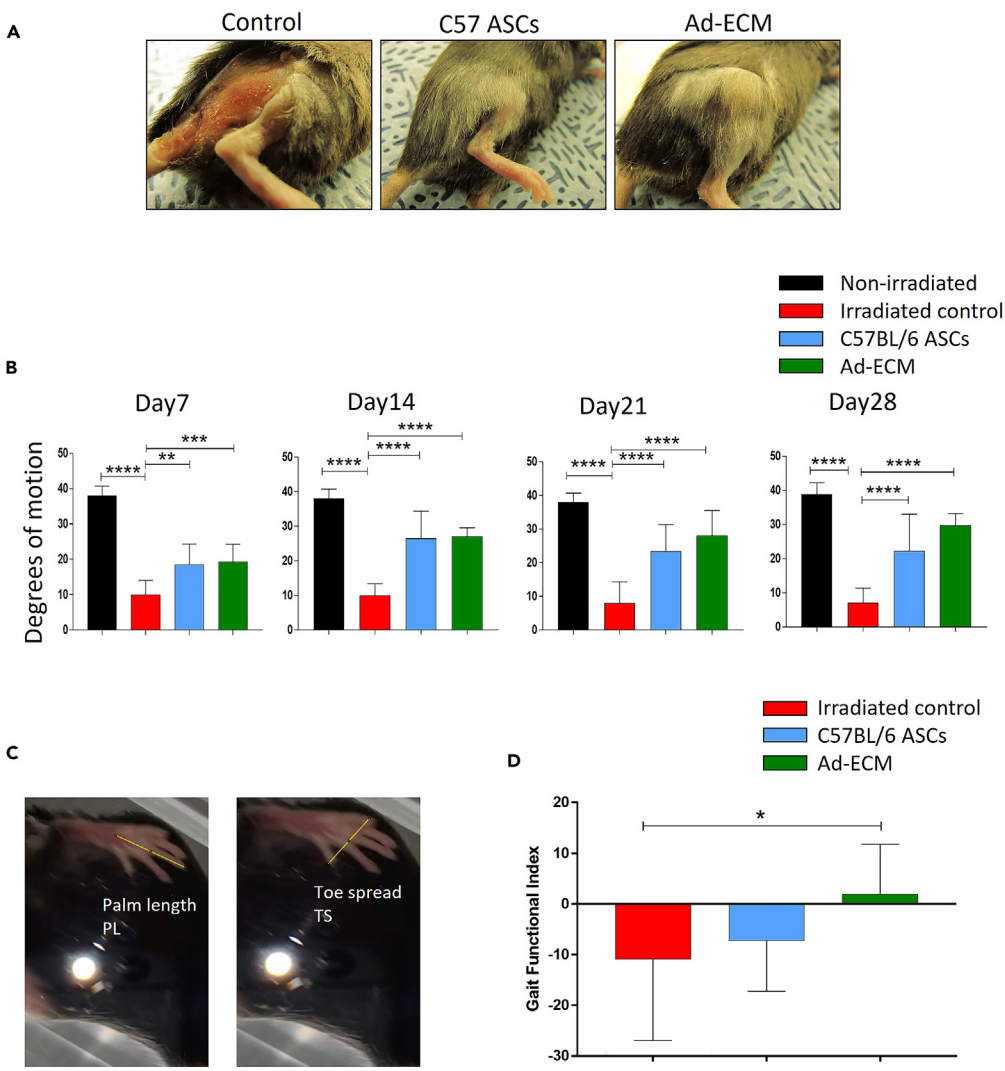

Figure 1. Impact of Ad-ECM therapy on functional outcomes linked to RISF

(A) Skin architecture at day 42 post 40 Gy irradiation. Local injection of 3 million ASCs or 200 ul Ad-ECM or saline (control) was performed on day 14 post-irradiation.

(B) The degree of leg motion was measured on days 7, 14, 21, and 28 post-treatment and plotted (n = 10).

(C and D) Palm length and toe spread were measured using ImageJ software, and values were used to calculate the gait functional index (n = 10). p value < 0.05 = *, <0.005 = **, <0.0005 = ***, <0.00005 = ****.

All data is reported as the mean ± standard deviation to assess the between-subject variability of the measured outcome.

non-obese diabetic (NOD)/severe combined immunodeficient (SCID) mice reduced skin injury and accelerated wound healing with a demonstration of hASCs migration to the site of radiation injury.[16,17] It is speculated that adipose-derived stem cells (ASCs) reduce fibrosis by antagonizing TGF-β pathway mediators via paracrine factors. We recently demonstrated that the hepatocyte growth factor secreted by ASCs mediate RISF in mice.[18] Although the use of adipose tissue components in the form of lipoaspirates has shown beneficial clinical outcomes in treating RISF, the highly invasive nature of the procedure involving aspiration of fat and injection at the irradiated site under anesthesia is one of the limiting factors. Secondly, due to the presence of living cells, including immune cells, lipoaspirate cannot be applied as an allogeneic approach due to the possibility of eliciting immune rejection or a host-versus-graft reaction.

ECM-based scaffolds developed from a variety of tissues, including human adipose tissue,[19] bone, dermis,[20] porcine dermis,[21] and urinary bladder,[22] have shown exceptional clinical promise as regenerative scaffolds. For example, porcine dermal ECM scaffolds contain a matrix that is primarily composed of collagen and elastin fibrils and glycosaminoglycans, structural proteins that are known to promote cellular attachment,[23] proliferation, and matrix reorganization.[24] Further, after decellularization of the porcine dermis, endogenous growth factors such as basic fibroblast growth factor and vascular endothelial growth factor, typically found within native tissue matrices, were preserved. ECM from different tissue sources has been successfully employed for regenerating volumetric muscle loss, temporomandibular joint defects,

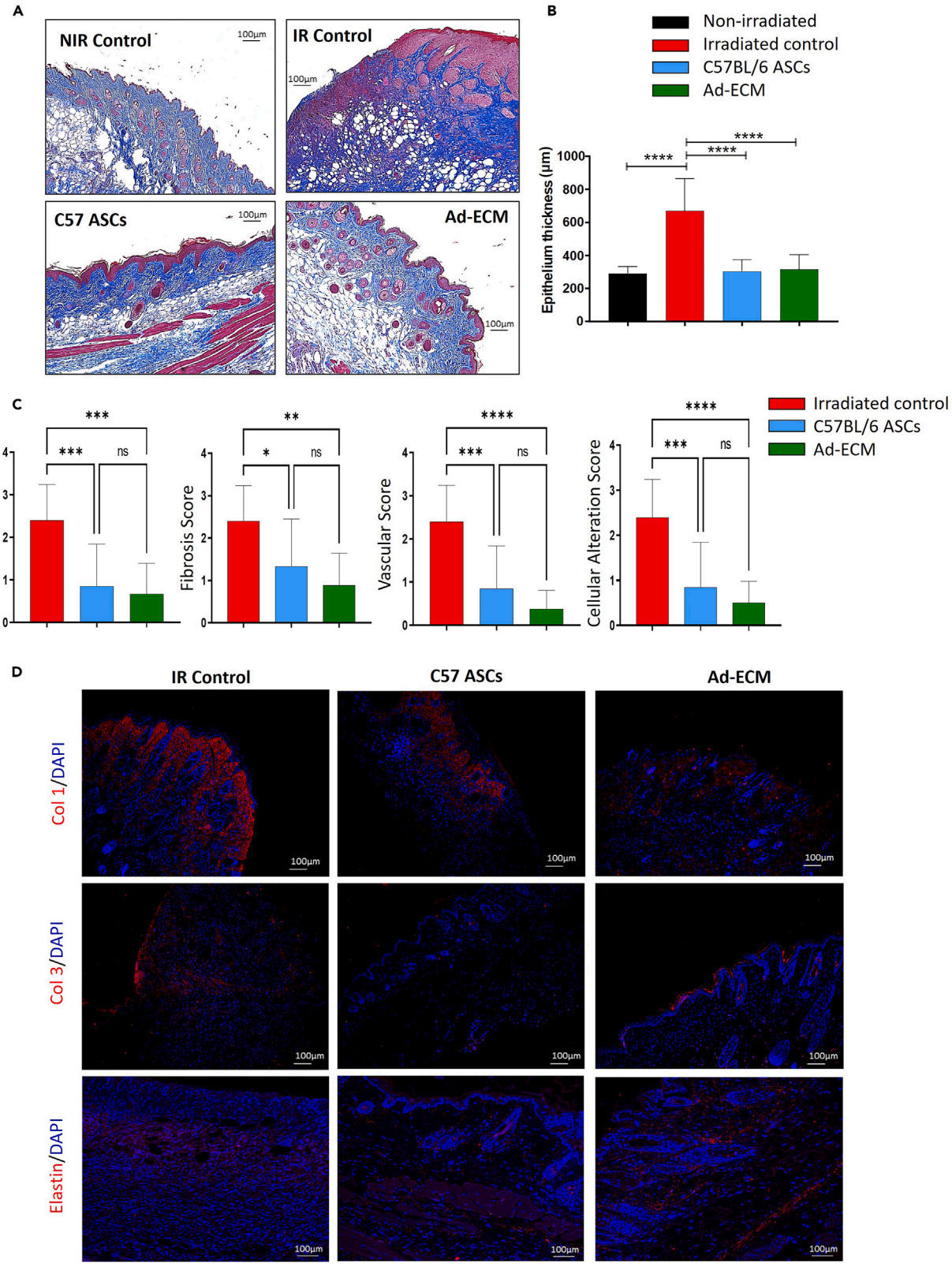
A
NIR Control
IR Control
C57 ASCs
Ad-ECM
100μm
B
Non-irradiated
Irradiated control
C57BL/6 ASCs
Ad-ECM
Epithelium thickness (μm)
****
C
Inflammation Score
Fibrosis Score
Vascular Score
Cellular Alteration Score
***
**
*
ns
D
IR Control
C57 ASCs
Ad-ECM
Col 1/DAPI
Col 3/DAPI
Elastin/DAPI

Figure 2. Impact of Ad-ECM therapy on histological outcomes linked to RISF

(A and B) Skin was surgically excised from a 40 Gy irradiated field, and histologically processed sections were stained with Masson's Trichrome stain (A). ImageJ software was applied to measure the epidermal and dermal thickness and plotted (B) (n = 10).

(C) Histologically stained sections were blindly scored for inflammation, fibrosis, vascularization, and cellular alteration. Scores were plotted (n = 10).

(D) Paraffin-fixed skin sections were stained for specific antibodies against Collagen 1, Collagen 3, and Elastin. p value < 0.05 = *, <0.005 = **, <0.0005 = ***, <0.00005 = ****.

All data is reported as the mean ± standard deviation to assess the between-subject variability of the measured outcome.

constructive modeling of partial-thickness defects, and reconstruction of the esophagus.[25] Host immune cells like macrophages play an important role in ECM-mediated regeneration processes. Studies have demonstrated modulation of host cellular response and phenotypic switch mediated by injected decellularized ECM.[26,27] In particular, decellularized ECM has been shown to promote a switch of M1 macrophages (inflammatory) to M2 (regenerative) macrophages within 7–14 days post-implantation.[25,27,28] In addition, scaffold materials composed of ECM are responsible for eliciting type 2 (Th2-type) immune response, a predominantly immunosuppressive and regenerative response associated with transplant acceptance.[29] Interleukins (ILs) like IL-4, IL-5, and IL-13 produced by resident tissue cells and migratory T cells play an important role in promoting macrophage phenotypic switch and eliciting Th2 immune response.[30]

This study evaluated the use of adipose-derived ECM (Ad-ECM) as a mitigator of RISF and analyzed the possible mechanism of amelioration.

RESULTS

Local Ad-ECM injection reduces skin and muscle fibrosis in irradiated hindlimbs

Our mouse model of radiation skin fibrosis involves 40 Gy focused irradiation to the hindlimb soft tissue of C57BL/6 mice, resulting in fibrotic tissue by histology[18,31]-restricted range of motion quantifiable by 30 days[18,31] and upregulation of fibrosis-related genes TGF-β, CTGF, tumor necrosis factor (TNF), IL-1, nuclear factor κB (NF-kB), and Col1-6.[18,31] Commercially available human Ad-ECM was obtained as an off-the-shelf product named Renuva (MTF Biologics, Edison, NJ). Local subcutaneous rigotomy and injection of 200 μL Ad-ECM on day 14 post-irradiation resulted in reduced soft tissue fibrosis, hair loss, and increased passive limb excursion movements within 4 weeks of treatment in irradiated C57BL/6 mice (Figures 1A, 1B, and S1). The magnitude of mitigation was comparable to the injection of autologous mouse ASCs which previously have shown successful mitigation (Figures 1A, 1B, and S1).[18] As a functional readout of mitigation, we monitored and recorded the capability of irradiated mice to spread their toes and put pressure on their palms while walking on a transparent track. Still images from the recorded videos were used to measure toe spread and palm length using ImageJ software. The gait functional index was calculated from the toe spread and palm length measures as published.[31,32] Results showed a significant improvement in gait function in Ad-ECM-injected mice (Figures 1C and 1D). Of note, we observed no side effects of injecting human-origin Ad-ECM in C57BL/6 mice.

Ad-ECM injection reduces epithelial thickness and collagen deposition and restores elastin levels in irradiated skin

Masson's Trichrome staining of irradiated skin histological sections revealed a significant decrease in dermal and epidermal thickness and collagen contents in Ad-ECM-injected mice (Figures 2A, 2B, and S2). ASCs injection also resulted in improvement in epithelium thickness post-irradiation. Blinded scoring of histological sections based on previously published guidelines[6] demonstrated significant improvement in inflammation, fibrosis, vascular, and cellular alteration scores in Ad-ECM-injected group (Figure 2C). Immunofluorescent staining for collagen 1 and 3 further corroborated Masson's Trichrome data. Ad-ECM-injected skin sections showed a notable reduction in collagen 1 and 3 stainings (Figure 2D). Irradiation results in the loss of elastin fibers resulting in reduced elasticity in the skin. Ad-ECM injection preserved elastin contents in irradiated skin indicating a preservation of skin elasticity (Figure 2D).

Ad-ECM reduces inflammation- and fibrosis-associated genes and protein expression in irradiated skin

Quantitative real-time PCR data from skin tissues revealed a significant downregulation of inflammatory genes (IL-1, IL-2, IL-6, NF-κB) and genes representative of fibrosis (collagen 1–6), upon Ad-ECM treatment of irradiated legs (Figures 3A–3J). Hypocellularity, inflammation, and fibrosis are the hallmark features of radiation-induced fibrosis.[6] Luminex screen of the irradiated skins revealed significant downregulation of hypocellularity-associated factors (GM-CSF, M-CSF, and G-CSF), inflammation factors (TNFα, IL-1, 6, and 17), and fibrosis-related factor TGF-β in Ad-ECM-treated mice (Figures 4A–4C). Autologous ASCs-injected mice also revealed the resolution of radiation injury-associated genes and proteins (Figures 3 and 4).

Ad-ECM treatment downregulates fibrosis and inflammation-related genes in irradiated human foreskin fibroblast (HFF) cells

We have previously published the use of irradiated HFF as a model for studying the effects of ASCs in regulating the expression of inflammation- and fibrosis-related genes.[18] The use of this model has enabled us to study the direct anti-fibrotic effect of a mitigator on radiated fibrosis-relevant cell type. Using the same model we studied the effects of Ad-ECM on the modulation of inflammatory (TNF, IL-6, NF-κB) and fibrosis-associated (collagen 1 and TGF-β) genes. A 10 Gy radiation dose resulted in the upregulation of genes in HFFs indicative of inflammation and fibrosis by day 4 post-irradiation as revealed by quantitative real-time PCR. Treatment of irradiated HFF cells with Ad-ECM 24 h after irradiation resulted in significant downregulation of inflammation and fibrosis genes (Figure 4D).

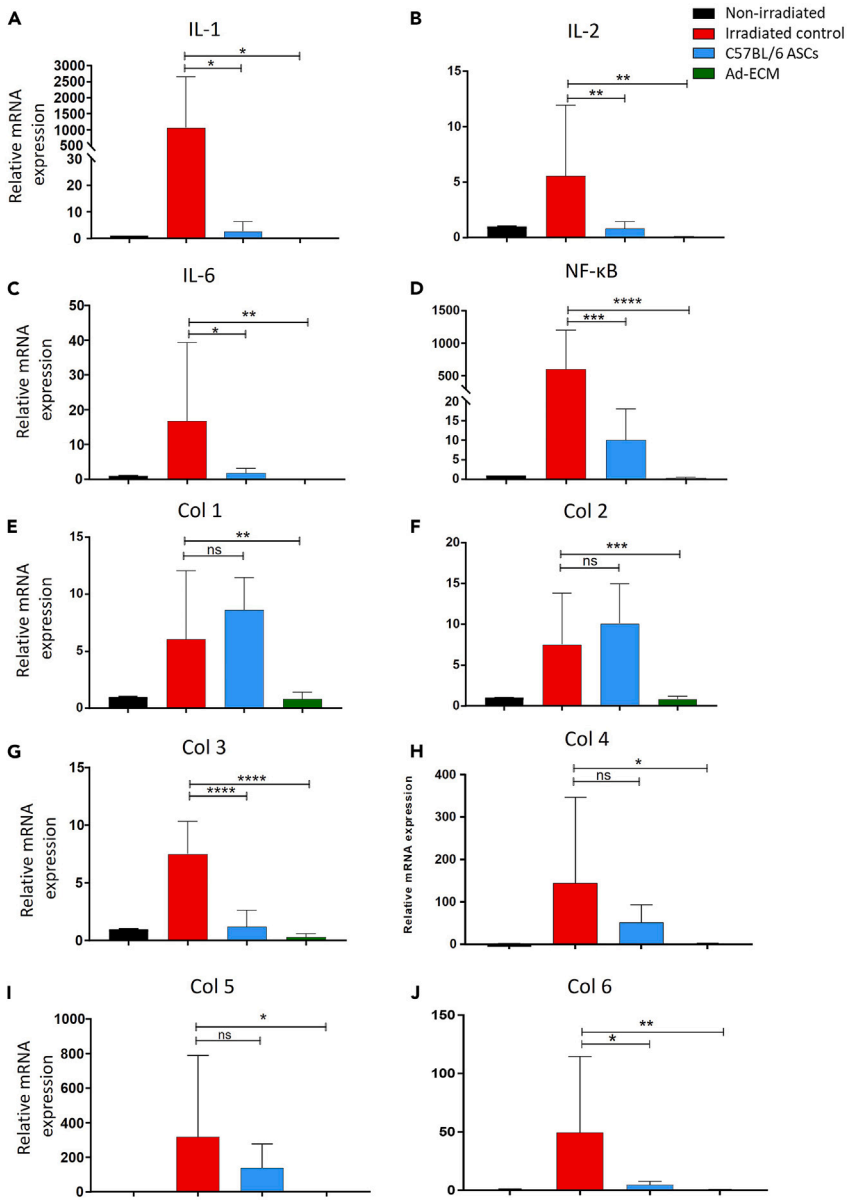

Figure 3. Ad-ECM therapy's influence on gene expression linked to RISF

(A–J) Expression of genes related to inflammation (A–D) (IL-1, IL-2, IL-6, and NF-B) and fibrosis (E–J) (Collagen 1–6) was analyzed in the skin of 40 Gy irradiated and differentially treated mice: non-irradiated, irradiated control, C57BL/6, and Ad-ECM on day 42 post-irradiation using real-time quantitative PCR (n = 5). p value < 0.05 = *, <0.005 = **, <0.0005 = ***, <0.00005 = ****.

All data is reported as the mean ± standard deviation to assess the between-subject variability of the measured outcome.

Ad-ECM injection in irradiated skin resulted in the upregulation of anti-inflammatory and regenerative cytokines involved in M2 macrophage polarization

The perpetual cycle of inflammatory and pro-fibrotic cytokines results in the development and establishment of fibrosis. The process of mitigation involves the dampening of inflammation and progression to regeneration. Luminex analyses of the irradiated skin injected with Ad-ECM showed upregulation of pro-regeneration protein MIG-2 (Figure 5A). In addition, our assay revealed upregulation of signature anti-inflammatory cytokines IL-4, IL-5, and IL-15 involved in the polarization of macrophages to regenerative M2 phenotype (Figures 5B and 5C).[33] M2 macrophages play an important role in wound healing and regeneration. To investigate the possible cell source responsible for producing IL-4, IL-5, and IL-15, we analyzed the histological sections of injected Ad-ECM. We observed homing of cells and the formation of vasculature within 4 weeks of injection (Figure 5D).

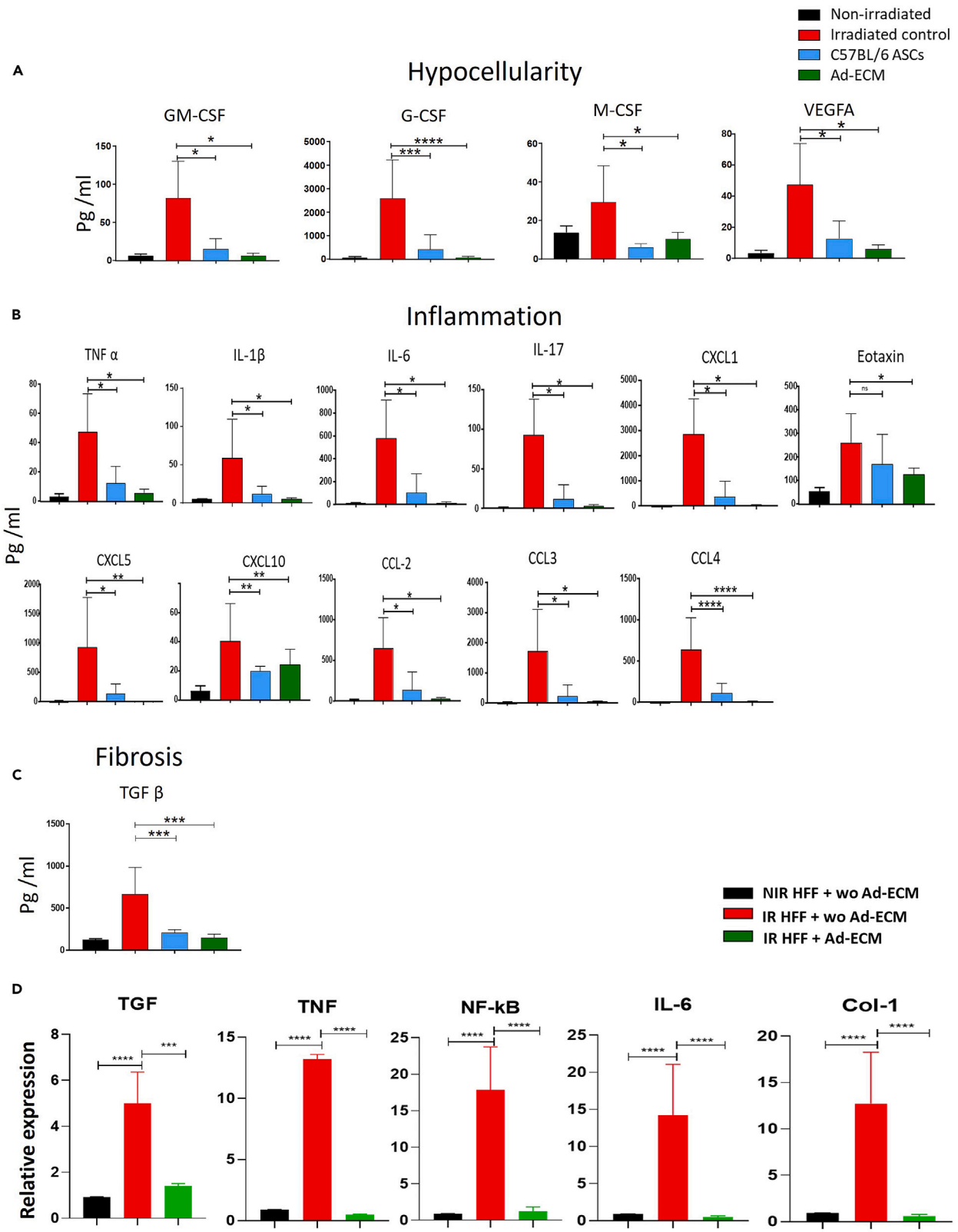
Non-irradiated
Irradiated control
C57BL/6 ASCs
Ad-ECM
A
Hypocellularity
GM-CSF
G-CSF
M-CSF
VEGFA
Pg /ml
B
Inflammation
TNF α
IL-1β
IL-6
IL-17
CXCL1
Eotaxin
CXCL5
CXCL10
CCL-2
CCL3
CCL4
Pg /ml
C
Fibrosis
TGF β
Pg /ml
NIR HFF + wo Ad-ECM
IR HFF + wo Ad-ECM
IR HFF + Ad-ECM
D
TGF
TNF
NF-kB
IL-6
Col-1
Relative expression

Figure 4. Ad-ECM therapy's influence on protein expression linked to RISF

(A–C) Expression of hypocellularity (A), Inflammation (B), and fibrosis (C) indicative proteins were analyzed in the skin of non-irradiated, 40 Gy irradiated control, -C57BL/6 ASCs and Ad-ECM-treated mice by Luminex technology at day 42 post-irradiation (n = 5).

(D) 10 Gy irradiated human foreskin fibroblasts were treated with Ad-ECM for 4 days. Expression of inflammation (TNF, IL-6, and NF-B) and fibrosis (TGF-β and Col 1) related genes were analyzed by quantitative real-time PCR (n = 3). p value < 0.05 = *, <0.005 = **, <0.0005 = ***, <0.00005 = ****.

All data is reported as the mean ± standard deviation to assess the between-subject variability of the measured outcome.

Ad-ECM treatment promotes endothelial cells migration and contributes to macrophage polarizing cytokines production

We have previously shown that adipose stem cells injection at the irradiated site enhances the migration of bone marrow cells to the irradiated tissue. To analyze whether Ad-ECM has a chemotactic effect, we analyzed bone marrow cell migration in a transwell culture where bone marrow isolated from GFP^+ mice was seeded in the transwell and Ad-ECM was added in the lower portion (Figure 5E). We observed a higher number of bone marrow cells migrated across the transwell membrane at day 6 post-culture (Figure 5F). To analyze cell types migrating to the Ad-ECM irradiated tissue we generated GFP^+ bone marrow chimeric mice and irradiated them with a single dose of 40 Gy. Ad-ECM was injected on day 14 post-irradiation, and skin samples were harvested on day 42 and analyzed by flow cytometry. Results revealed a higher number of endothelial cells and macrophages from bone marrow migrated from the bone marrow cells (Figure 5G). The irradiated wound was enriched with fibroblasts, and we observed migration of endothelial cells upon Ad-ECM injection. To analyze the role of these two cell types as a possible source of M2 cytokines production, we subjected fibroblasts and endothelial cells (HUVECs) to Ad-ECM digest.[34] We observed a strong dose-dependent upregulation of IL-4, IL-5, and IL-15 gene expression in endothelial cells (Figure 5H). Although fibroblasts also showed upregulated expression, the magnitude was approximately 100-fold lower than that of the endothelial cells (Figure 5H). We concluded that Ad-ECM treatment promotes bone marrow cell migration, mainly endothelial and macrophages to the irradiated site, and most likely these endothelial cells prime the environment for M2 macrophage polarization by promoting IL-4 and IL-5 production.

Ad-ECM retains growth factors that possibly promote vascularization and inhibit fibrosis

To determine what growth factors are retained in Ad-ECM, we focused on factors reported in the literature for having a direct inhibitory effect on fibrosis genes and factors that promote vascularization as hypoxia is one of the main drivers of the fibrosis process. We have previously shown the presence of insulin growth factor (IGF)-1, VEGF, fibroblast growth factor (FGF)-1, FGF-2, and epidermal growth factor (EGF) in Ad-ECM.[35] HGF plays an important role in the mitigation of radiation-induced fibrosis.[31] We confirmed the presence of HGF in Ad-ECM by ELISA (Figures S3A and S3B). We further confirm the role of HGF in the reduction of fibrosis by performing transwell co-cultures. Co-culture of irradiated fibroblasts with wild-type ASCs results in downregulation of TGF-β expression in irradiated fibroblasts (Figure S3C). However, the co-culture of irradiated fibroblasts with ASCs isolated from HGF conditional knockout mice failed to down-modulate pro-fibrotic gene TGF-β (Figure S3C). These results indicated that retention of these growth factors plays an important role in the mitigation by Ad-ECM.

Prophylactic use of Ad-ECM can mitigate chronic phase fibrosis development in mice

Early application of Ad-ECM post-radiation exposure might be a beneficial mitigation strategy to block the development of chronic fibrosis post-radiation exposure from oncological treatment-related, accidental, or terroristic exposure. To act as a possible countermeasure agent, the capability of Ad-ECM to mitigate fibrosis upon early application is a crucial feature. To analyze whether Ad-ECM can be used for prophylaxis, we injected Ad-ECM 2 days before irradiation or 1-day post-irradiation and compared these time points to the 14 days post-irradiation application regime. Based on our previous studies showing the beneficial effects of ASCs in mitigating fibrosis via HGF secretion,[31] we tested a combination therapy approach consisting of Ad-ECM plus HGF or Ad-ECM plus autologous ASCs at day 14 post-irradiation. Results revealed a visible improvement of skin in all the treatment approaches (Figures 6A and S4). Although pre-exposure or 1-day post-exposure approaches were not able to block the acute wound, treated mice were protected from late irradiation side effects. The functional outcome of a limb excursion readout showed a significant improvement in all treated groups (Figure 6B). We observed an enhanced improvement in limb excursion in both Ad-ECM plus HGF ($p = 0.0051$)- and Ad-ECM plus ASCs ($p = 0.0030$)-treated mice groups, but the magnitude was not significantly better than that of Ad-ECM alone ($p = 0.0058$) (Figure 6B).

Mice treated with Ad-ECM in the early phase of irradiation exposure showed improved skin histology, lower collagen deposition, and inflammation

We analyzed the skin of the irradiated mice treated at different time points post-exposure with Ad-ECM alone or as a combination therapy. Masson's Trichrome staining of the histology sections revealed lower collagen deposition (Figures 6C and S5). Control PBS-treated mice showed thickened epithelium, while Ad-ECM-treated mice's epithelium thickness was comparable to normal non-irradiated skin (Figure 6D). Ad-ECM-treated mice skin scored significantly better for inflammation, fibrosis, vascular, and cellular alteration index (Figure 6E). Immunofluorescence staining of collagen 1 (Figure 7A) and collagen 3 (Figure 7B) confirmed lower deposition in Ad-ECM-treated mice. Real-time PCR results showed upregulation of inflammation (IL-1 and IL-6) and fibrosis-related genes (TGF-β and collagen 1–6) (Figure 7C). As one of the potential applications of Ad-ECM is for the treatment of RISF in irradiated oncological fields, we tested the oncological safety of Ad-ECM by incubating it with well-established breast cancer tumor cell lines MCF-7 and MDA-MB-231.[36] MCF-7 or MDA-MB-231 cells were cultured

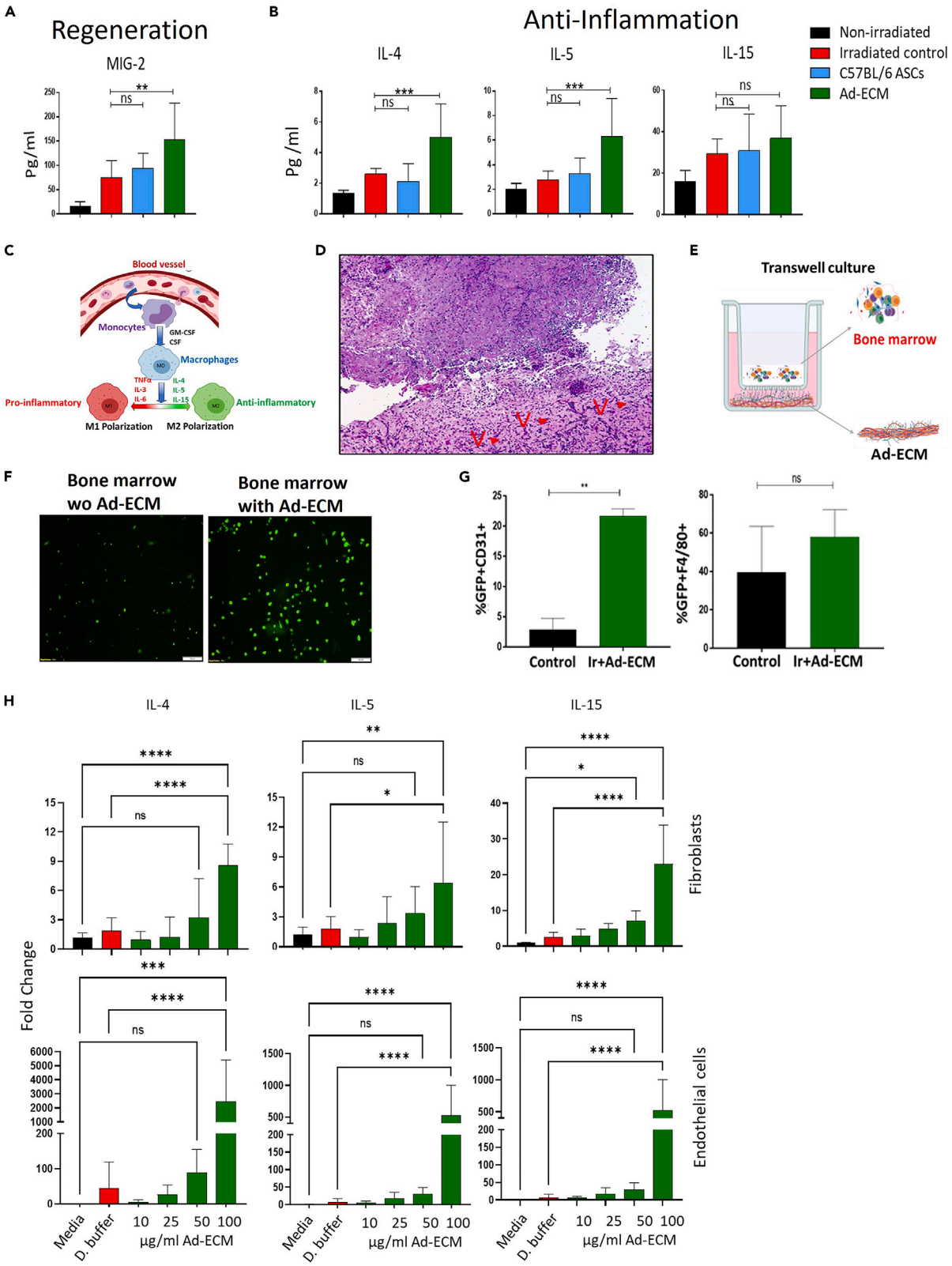
A
Regeneration
MIG-2
Pg/ml
B
Anti-Inflammation
IL-4
IL-5
IL-15
Pg /ml
Non-irradiated
Irradiated control
C57BL/6 ASCs
Ad-ECM
C
Blood vessel
Monocytes
GM-CSF
CSF
Macrophages
TNFα
IL-3
IL-6
IL-4
IL-5
IL-15
Pro-inflammatory
Anti-inflammatory
M1 Polarization
M2 Polarization
D
E
Transwell culture
Bone marrow
Ad-ECM
F
Bone marrow
wo Ad-ECM
Bone marrow
with Ad-ECM
G
%GFP+CD31+
%GFP+F4/80+
Control
Ir+Ad-ECM
H
IL-4
IL-5
IL-15
Fibroblasts
Endothelial cells
Fold Change
Media
D. buffer
10
25
50
100
µg/ml Ad-ECM

Figure 5. Effect of Ad-ECM therapy on M2 macrophage polarization

(A and B) Expression of MIG-2 and (B) anti-inflammation (IL-4, IL-5, and IL-15) proteins were analyzed in the skin 40 Gy irradiated mice groups at day 42 post-irradiation by Luminex assay (n = 5).

(C) Schematic of macrophage polarization to M1 and M2 phenotypes.

(D) Ad-ECM injected subcutaneously in the 40 Gy irradiated field was surgically excised and histologically processed to obtain thin sections and stained with H&E stain. Newly formed vessels are indicated with red arrows.

(E) Schematic of bone marrow migration using a transwell culture setup.

(F) Bone marrow cells isolated from GFP^+ mice were co-cultured with Ad-ECM. Migrated GFP^+ cells were visualized under a fluorescent microscope.

(G) GFP^+ bone marrow chimeric mice were irradiated using a 40 Gy irradiation dose and injected with Ad-ECM on day 14 post-irradiation. Skin was surgically excised, and single-cell suspension was generated by dispase and collagenase digestion. Single-cell suspension was analyzed by flow cytometry for expression of $CD31^+$ and $F4/80^+$ cells by gating on the GFP^+ population (n = 5).

(H) Endothelial cells (HUVECs) or fibroblasts were grown to full confluency and treated with increasing doses of digested Ad-ECM. Cells were lysed using RNA lysis buffer after 4 days, and expression of IL-4, IL-5, and IL-15 was determined using quantitative real-time qPCR (n = 3). p value < 0.05 = *, <0.005 = **, <0.0005 = ***, <0.00005 = ****.

All data is reported as the mean ± standard deviation to assess the between-subject variability of the measured outcome.

in the presence of 50 μg/ml Ad-ECM digest for 4 days. Cell count using the Neubauer chamber revealed no significant effect on cell proliferation in Ad-ECM cultured group compared to control (Figure 7D).

DISCUSSION

Autologous fat grafting has been used as a tool to successfully mitigate RISF. Autologous fat grafts enriched with ASCs are routinely used for reconstructive surgical procedures.[37,38] There has been published clinical evidence demonstrating the beneficial use of autologous fat for the treatment of radiotherapy-induced tissue damage.[32] These data report an improvement in fibrosis and LENT-SOMA score attributed to enhanced vascularization and hydration of fibrotic tissue, an outcome mainly mediated by ASCs.[39] Subsequent studies verified the initial observations and an improvement in skin texture, and softening of fibrotic tissue was observed in childhood facial cancer treatment trials.[40–42] The mitigation effects are attributed to the anti-inflammatory and regenerative cytokines produced by the ASCs residing in the adipose tissue. Many of these cytokines become integrated into the cytoskeleton of the adipose tissue. The presence of the immune system activating components and immune cells in the adipose tissue restricts its application to an autologous approach to avoid immune rejection or host-versus-graft reaction. Harvesting of autologous fat is a traumatic procedure and often requires full anesthesia. In addition, the availability of harvestable fat at times in cancer patients is challenging due to lifestyle changes and disease progression. Furthermore, the application of autologous fat as a mitigator in accidental situations of radiation exposure is not feasible. Human Ad-ECM has been used in clinics as an esthetic filler and has been shown to promote vascularization and stem cell differentiation.[19,35] In previous studies conducted in nude mice and humans, we observed no local or systemic side effects of Ad-ECM treatment.[19,35] In addition, Ad-ECM is routinely used in clinics as a filler material in an allogeneic approach without any clinical complications arising from the procedure. Furthermore, Ad-ECM retains many of the growth factors post-processing present in adipose tissue.[35]

In the present study, we evaluated the utilization of Ad-ECM as a mitigator of RISF and studied the possible mechanisms of mitigation. We utilized a mouse model of RISF[31] to determine the role of Ad-ECM injection in the process of RISF management. We measured fibrosis in irradiated tissue using histological and molecular analysis. There was thickening of skin epithelium, edema, influx of inflammatory cells to irradiated sites, and upregulated expression of TGF-β and collagens I–IV in irradiated skin tissue. The functional readout of the RISF was a loss of limb excursion and reduction in the gait index. Injection of Ad-ECM at day 14 post-irradiation resulted in significant improvement in the clinical, histological, and molecular signature of RISF. We observed improvement in skin appearance, hair regrowth, limb excursion, and gait. We have previously shown the successful use of ASCs to mitigate RISF.[43] We employed ASCs as a positive comparative control to estimate the magnitude of Ad-ECM mitigation. We observed that Ad-ECM showed comparable mitigation to ASCs. A recent clinical evaluation of Ad-ECM showed a beneficial effect on patients in alleviating RISF.[44]

Histological evaluation of the Ad-ECM-treated skin sections showed a decrease in epithelium thickening, inflammation, and collagen deposition. We also observed more elastin expression indicating recovery of skin elasticity. Studies have shown the beneficial effect of restoring elastin expression on the outcome of RISF.[45] At the molecular level, Ad-ECM treatment resulted in a reduction of pro-inflammatory and fibrosis gene and protein expression. Reduction of inflammation and fibrosis-eliciting factors is critical to prevent the progression of RISF.[46] Our co-culture studies revealed Ad-ECM can directly lower the expression of inflammation and fibrotic genes in irradiated fibroblasts. Most likely this effect is mediated by the growth factors retained in the Ad-ECM. We have previously shown the role of HGF in the mitigation of RISF.[18] Analysis of Ad-ECM by ELISA confirmed the retention of HGF. ASCs residing in the adipose tissue are known for secreting a plethora of paracrine factors like IL-10, bFGF, VEGF, and TGF-β-3 upon stimulation. These factors along with HGF have been shown to exert anti-fibrotic effects involved in the attenuation of myocardial, pulmonary, hepatic, and renal fibrosis.[47] Previous studies have shown the presence of these factors in Ad-ECM.[35,44] Our *in vitro* co-culture studies revealed HGF plays a key role in dampening TGFβ expression, but it is most likely that the anti-fibrotic effects of Ad-ECM therapy are exerted by more than one paracrine factor. Furthermore, our *in vivo* irradiation of GFP^+LUC^+ bone marrow chimeric mice indicated a likely role of Ad-ECM to promote the migration of bone marrow cells to the irradiated site. Previous studies have demonstrated the role of the HGF-*c*-met axis in promoting the migration of bone marrow-origin $CD45^+$ cells to skeletal muscle.[48]

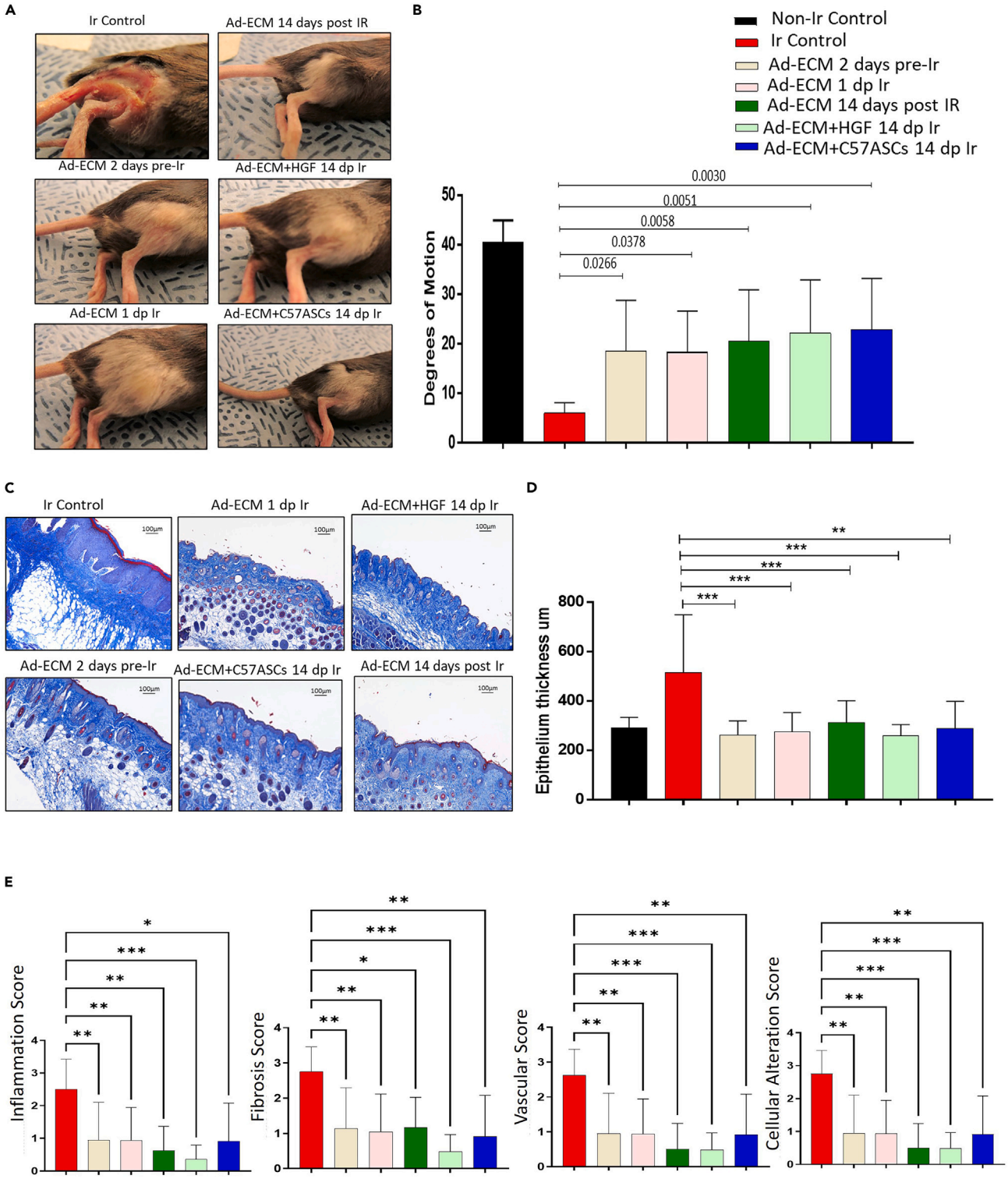

Figure 6. Prophylactic use of Ad-ECM therapy

(A) C57BL/6 mice were 40 Gy irradiated at the hindlimb. Mice were treated with PBS control (Ir Control), Ad-ECM 2 days before irradiation (Ad-ECM 2 days pre-Ir), Ad-ECM 1 day post-irradiation (Ad-ECM 1dp Ir), Ad-ECM 14 days post-Irradiation, Ad-ECM+5μg HGF 14 days post-irradiation or Ad-ECM+ 3 × 10^6 C57ASCs 14 days post-irradiation. Skin architecture at day 42 post-irradiation.

(B) The degree of leg motion was measured on day 28 post-treatment and plotted (n = 8).

Figure 6. *Continued*

(C and D) Skin was surgically excised from a 40 Gy irradiated field, and histologically processed sections were stained with Masson's Trichrome stain (C). ImageJ software was applied to measure the epithelium thickness and plotted (D) (n = 8).

(E) Histologically stained sections were blindly scored for inflammation, fibrosis, vascularization, and cellular alteration. Scores were plotted (n = 8). p value < 0.05 = *, <0.005 = **, <0.0005 = ***, <0.00005 = ****.

All data is reported as the mean ± standard deviation to assess the between-subject variability of the measured outcome.

Studies in rats showed initial inflammation followed by the development of fibrosis, characterized by thickening of epithelium, frequent necrosis, and deposition of collagen.[6] Previous studies have shown the involvement of HGF in increased vascularization,[49] decreased inflammation,[50] downregulation of the pro-fibrotic TGF-β-Smad signaling pathway,[51] and promoting migration of bone marrow-resident tissue-specific progenitor cells.[48]

Macrophages play an important role in maintaining immune homeostasis and can modify their phenotype to inflammatory (M1) or regenerative (M2) based on the microenvironment.[52] Pro-inflammatory macrophages play an important role in the acute phase of wound healing by calling in helper cells, and in the later phase of healing regenerative M2 macrophages are the key. IL-4, IL-5, and IL-15 are the key players in polarizing macrophages to the M2 phenotype.[52] Our Luminex screen of the irradiated Ad-ECM-treated skin revealed higher production of pro-M2 polarizing cytokines production. M2 macrophages release anti-inflammatory factors that indicate the most plausible explanation of dampening inflammation in Ad-ECM-treated skin. Our cell tracing studies indicated an increased influx of macrophages and endothelial cells in response to Ad-ECM injection. Endothelial cells play an important role in neovascularization that results in a reduction of hypoxia. We observed increased vascularization of the injected Ad-ECM. In addition, the treatment of endothelial cells with Ad-ECM resulted in the upregulation of the M2 polarization genes. These results indicate that endothelial cells play an important role in mitigation via neovascularization and by promoting M2 macrophage polarization. Matrix metalloproteinases (MMPs) contribute to maintain a balance between ECM generation and degradation. In fibrosis this balance is deregulated. Macrophages are the main producers of MMP and thus can contribute to fibrosis reduction via restoring the ECM balance. As the mechanism of RISF development overlaps with the mechanism(s) involved in development of scars from other injuries (burn, trauma etc), the outcome of Ad-ECM application in RISF management advocates for potential testing as mitigator for other conditions resulting in scar formation.

RISF is also the aftermath of exposure to radiation from industrial accidents, war, or terroristic activities. The threat of such incidents has intensified due to the increased use of radioactive materials in the industry and military installations.[53] Ad-ECM is available as an off-the-shelf product. Therefore it has great potential to be used as a countermeasure for RISF. An important clinical scenario for radiation therapy is to investigate the prophylactic use of agents to prevent the establishment of RISF in the first place. In this study, we evaluated both prophylactic use (i.e., 2 days before irradiation) and early time point post-irradiation (i.e., 1 day after irradiation). Both these regimens prevented late fibrosis development but failed to protect from early injury and edema. Previous studies have shown the benefits of using ASCs alone or in combination with autologous fat as a mitigator of RISF. We have demonstrated the role of HGF produced by ASCs as one of the key players in the mitigation process. The logical question was whether enrichment of Ad-ECM with ASCs or HGF can improve the outcome of RISF treatment. We tested both these combinations and observed that a combination of Ad-ECM and ASCs gives the best functional outcome. Further, higher and lower doses of HGF need to be investigated to get an optimal outcome.

In addition to adipose tissue, ECM from other tissue sources has also been explored for the treatment of radiation-induced fibrosis. For example, bladder-derived matrix (BDM) has shown promising results in preclinical studies. BDM contains unique components that can modulate the fibrotic response and promote tissue regeneration. Studies have demonstrated its ability to reduce fibrosis and improve tissue function in animal models of radiation-induced bladder fibrosis.[54] Similarly, dermal-derived ECM has shown potential for treating RISF. Dermal ECM provides a supportive environment for cell growth, migration, and tissue regeneration. It has been investigated in animal models and clinical studies, showing improvements in skin texture, elasticity, and reduced fibrosis.[55,56] The choice of ECM source depends on the specific tissue affected by radiation-induced fibrosis. Each ECM type possesses its unique composition and growth factor profile, which can influence the therapeutic outcomes. Furthermore, the availability and ease of extraction of ECM from different tissue sources should be considered for clinical translation. Further research is ongoing to optimize the use of ECM from various tissue types for the treatment of radiation-induced fibrosis. This includes investigating the specific mechanisms by which ECM modulates the fibrotic response, refining the delivery methods, and assessing long-term efficacy and safety in larger patient populations.

Although initial studies have shown no adverse effects in patients upon Ad-ECM application[19] and our *in vitro* co-culture studies using breast cancer cell lines also reflected no enhancement in proliferation of the cancer cells indicating a non-oncogenic character of Ad-ECm, further *in vivo* studies are required to establish the safety profile of the Ad-ECM application in a potential oncological field. How cancer cells and cancer stem cells behave in the presence of Ad-ECM needs to be investigated. In addition, high-throughput studies are required to analyze the composition of Ad-ECM and single out the component(s) responsible for mitigation and their mitigation concentration.

Limitations of the study

In this study, we examined the impact of Ad-ECM on mitigating RISF and explored the potential mechanisms underlying this mitigation. Our findings suggest that a shift toward the regenerative M2 phenotype in macrophages may be a key mechanism. While this study offers insights into potential factors involved, more comprehensive studies employing macrophage elimination and adoptive transfers are required. Additionally, single-cell analytics are crucial to pinpoint other cell populations that release cytokines, driving the polarization of M2 macrophages.

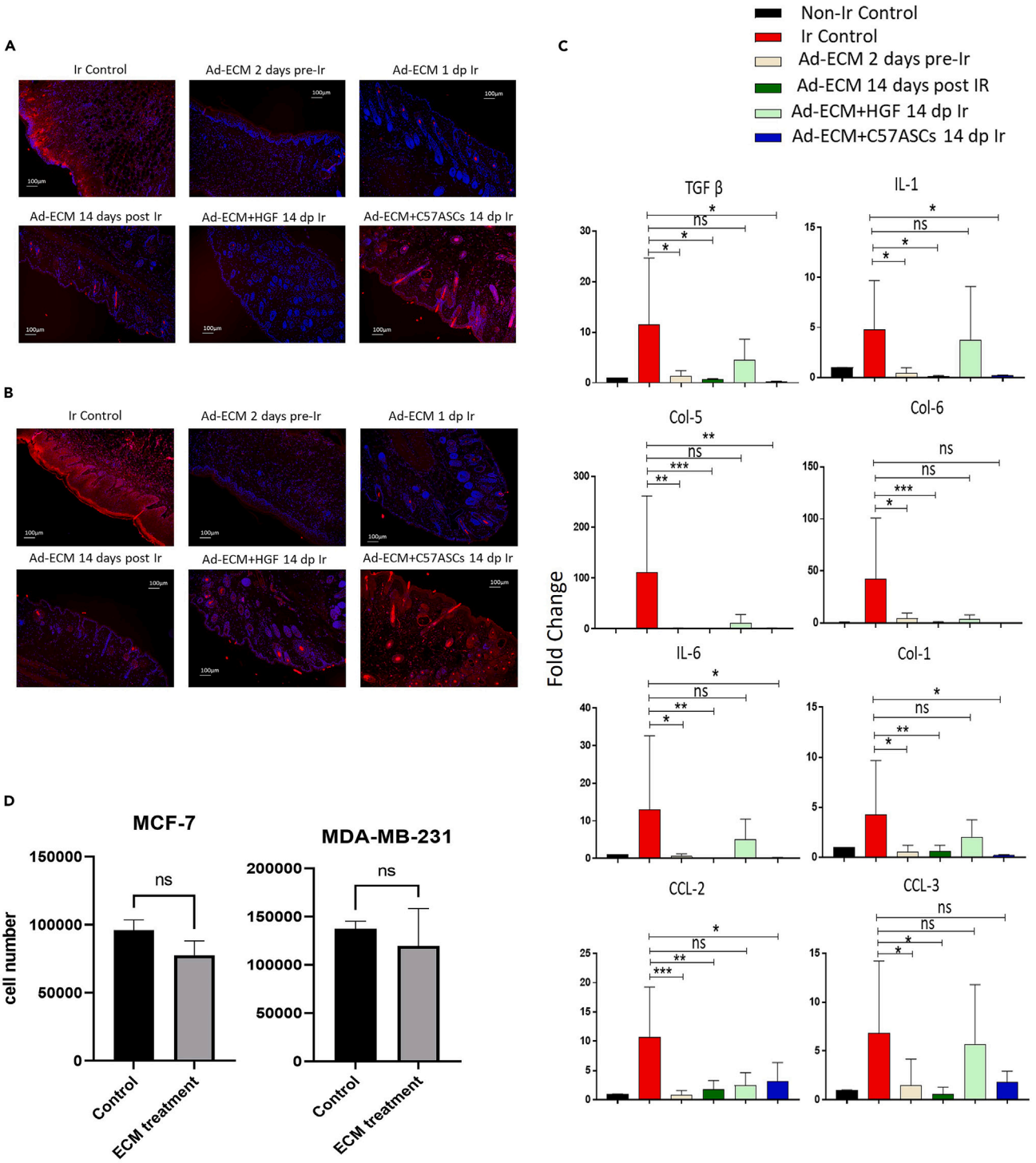

Figure 7. Impact of prophylactic Ad-ECM therapy on histological outcomes linked to RISF

(A and B) Paraffin-fixed skin sections were stained for specific antibodies against Collagen 1 (A) and Collagen 3 (B).

(C) Expression of genes related to inflammation (A-D) (IL-1, IL-6, CCL-2, CCL-3) and fibrosis (TGF-β, Collagen 1, 5, and 6) was analyzed in the skin of 40 Gy irradiated using real-time quantitative PCR (n = 5).

(D) $5x10^4$ MSF-7 or MDA-MB-231 cells were incubated with Ad-ECM solution 50 μg/mL for 4 days in 6 well plates. Control wells were incubated with buffer control. Trypsinized cells were counted using Neubauer chamber and plotted. p value < 0.05 = *, <0.005 = **, <0.0005 = ***, <0.00005 = ****, ns = non-significant. All data is reported as the mean ± standard deviation to assess the between-subject variability of the measured outcome.

STAR★METHODS

Detailed methods are provided in the online version of this paper and include the following:

- KEY RESOURCES TABLE
- RESOURCE AVAILABILITY
  - Lead contact
  - Materials availability
  - Data and code availability
- EXPERIMENTAL MODEL AND STUDY PARTICIPANT DETAILS
- METHOD DETAILS
  - Adipose-derived extracellular matrix
  - Leg contracture measurements
  - Measurement of gait functional index
  - Histological evaluation of skin damage and collagen deposition
  - Immunofluorescence staining
  - Isolation of adipose-derived stem cells
  - Chimeric mice generation
  - Transwell co-culture
  - Real-time PCR
  - Luminex assay
  - Digestion of Ad-ECM
- QUANTIFICATION AND STATISTICAL ANALYSIS

SUPPLEMENTAL INFORMATION

Supplemental information can be found online at https://doi.org/10.1016/j.isci.2023.107660.

ACKNOWLEDGMENTS

This study was supported by DOD Grant W81XWH-19-PRMRP-DA, NIH/NIAID grant 5R21AI153971-02, and PSF/MTF grant to A.E.
We would like to express our gratitude to Dr. George Michalopoulos and Dr. Wendy Michelle Mars for providing us with HGF floxed mice.

AUTHOR CONTRIBUTIONS

S.C.: collection and assembly of data, data analysis and interpretation; K.S.Y.: collection of data; data analysis; Y.S.: collection of data, data analysis; F.B.: collection of data, data analysis; J.A.: collection of data; Z.T.: collection of data; H.M.: collection of data; M.W.E.: collection and assembly of data, data analysis and interpretation; J.S.G.: conception and design, data interpretation; P.J.R.: conception and design, data analysis and interpretation; A.E.: conception and design, collection and assembly of data, data analysis and interpretation, manuscript writing and final approval.

DECLARATION OF INTERESTS

The authors declare no competing interests.

Received: March 28, 2023
Revised: June 30, 2023
Accepted: August 15, 2023
Published: August 17, 2023

REFERENCES

1. Barton, M.B., Jacob, S., Shafiq, J., Wong, K., Thompson, S.R., Hanna, T.P., and Delaney, G.P. (2014). Estimating the demand for radiotherapy from the evidence: a review of changes from 2003 to 2012. Radiother. Oncol. *112*, 140–144.
2. Jaffray, D.A., and Gospodarowicz, M.K. (2015). Radiation therapy for cancer. Cancer Dis. Control Priorities *3*, 239–248.
3. Dangwal, S., Stratmann, B., Bang, C., Lorenzen, J.M., Kumarswamy, R., Fiedler, J., Falk, C.S., Scholz, C.J., Thum, T., and Tschoepe, D. (2015). Impairment of Wound Healing in Patients With Type 2 Diabetes Mellitus Influences Circulating MicroRNA Patterns via Inflammatory CytokinesSignificance. Arterioscler. Thromb. Vasc. Biol. *35*, 1480–1488.
4. Arcangeli, G., Friedman, M., and Paoluzi, R. (1974). A quantitative study of late radiation effect on normal skin and subcutaneous tissues in human beings. Br. J. Radiol. *47*, 44–50. https://doi.org/10.1259/0007-1285-47-553-44.
5. Jones, R.E., Foster, D.S., Hu, M.S., and Longaker, M.T. (2019). Wound healing and fibrosis: current stem cell therapies. Transfusion *59*, 884–892.
6. Gallet, P., Phulpin, B., Merlin, J.-L., Leroux, A., Bravetti, P., Mecellem, H., Tran, N., and Dolivet, G. (2011). Long-term alterations of cytokines and growth factors expression in irradiated tissues and relation with histological severity scoring. PLoS One *6*, e29399.
7. Abraham, D.J., Eckes, B., Rajkumar, V., and Krieg, T. (2007). New developments in fibroblast and myofibroblast biology: implications for fibrosis and scleroderma. Curr. Rheumatol. Rep. *9*, 136–143.
8. Kumar, V. (2005). Tissue renewal and repair: regeneration, healing, and fibrosis. In

Pathologic Basis of Disease, V. Kumar, A.K. Abbas, and N. Fausto, eds. (Elsevier), pp. 87–118.
9. Bentzen, S.M. (2006). Preventing or reducing late side effects of radiation therapy: radiobiology meets molecular pathology. Nat. Rev. Cancer *6*, 702–713.
10. Martin, M., Lefaix, J., and Delanian, S. (2000). TGF-β1 and radiation fibrosis: a master switch and a specific therapeutic target? Int. J. Radiat. Oncol. Biol. Phys. *47*, 277–290.
11. Ehrhart, E.J., Segarini, P., Tsang, M.L., Carroll, A.G., and Barcellos-Hoff, M.-H. (1997). Latent transforming growth factor beta1 activation *in situ*: quantitative and functional evidence after low-dose gamma-irradiation. Faseb. J. *11*, 991–1002.
12. Leask, A., and Abraham, D.J. (2004). TGF-β signaling and the fibrotic response. Faseb. J. *18*, 816–827.
13. Schultze-Mosgau, S., Blaese, M.A., Grabenbauer, G., Wehrhan, F., Kopp, J., Amann, K., Rodemann, H.P., and Rödel, F. (2004). Smad-3 and Smad-7 Expression following Anti-Transforming Growth Factor beta 1 (TGFβ1)-treatment in irradiated rat tissue. Radiother. Oncol. *70*, 249–259.
14. Shukla, L., Morrison, W.A., and Shayan, R. (2015). Adipose-derived stem cells in radiotherapy injury: a new frontier. Front. Surg. *2*, 1. https://doi.org/10.3389/fsurg.2015.00001.
15. Rigotti, G., Marchi, A., Galiè, M., Baroni, G., Benati, D., Krampera, M., Pasini, A., and Sbarbati, A. (2007). Clinical treatment of radiotherapy tissue damage by lipoaspirate transplant: a healing process mediated by adipose-derived adult stem cells. Plast. Reconstr. Surg. *119*, 1409–1422. , discussion 1423-1404. https://doi.org/10.1097/01.prs.0000256047.47909.71.
16. Sultan, S.M., Stern, C.S., Allen, R.J., Jr., Thanik, V.D., Chang, C.C., Nguyen, P.D., Canizares, O., Szpalski, C., Saadeh, P.B., Warren, S.M., et al. (2011). Human fat grafting alleviates radiation skin damage in a murine model. Plast. Reconstr. Surg. *128*, 363–372. https://doi.org/10.1097/PRS.0b013e31821e6e90.
17. Garza, R.M., Paik, K.J., Chung, M.T., Duscher, D., Gurtner, G.C., Longaker, M.T., and Wan, D.C. (2014). Studies in fat grafting: Part III. Fat grafting irradiated tissue–improved skin quality and decreased fat graft retention. Plast. Reconstr. Surg. *134*, 249–257. https://doi.org/10.1097/PRS.0000000000000326.
18. Ejaz, A., Epperly, M.W., Hou, W., Greenberger, J.S., and Rubin, J.P. (2019). Adipose-derived stem cell therapy ameliorates ionizing irradiation fibrosis via hepatocyte growth factor-mediated transforming growth factor-β downregulation and recruitment of bone marrow cells. Stem Cell. *37*, 791–802.
19. Kokai, L.E., Sivak, W.N., Schilling, B.K., Karunamurthy, A., Egro, F.M., Schusterman, M.A., Minteer, D.M., Simon, P., D'Amico, R.A., and Rubin, J.P. (2020). Clinical evaluation of an off-the-shelf allogeneic adipose matrix for soft tissue reconstruction. Plast. Reconstr. Surg. Glob. Open *8*, e2574.
20. Shepherd, N., Greenwell, H., Hill, M., Vidal, R., and Scheetz, J.P. (2009). Root Coverage Using Acellular Dermal Matrix and Comparing a Coronally Positioned Tunnel With and Without Platelet-Rich Plasma: A Pilot Study in Humans. J. Periodontol. *80*, 397–404.
21. Reing, J.E., Brown, B.N., Daly, K.A., Freund, J.M., Gilbert, T.W., Hsiong, S.X., Huber, A., Kullas, K.E., Tottey, S., Wolf, M.T., and Badylak, S.F. (2010). The effects of processing methods upon mechanical and biologic properties of porcine dermal extracellular matrix scaffolds. Biomaterials *31*, 8626–8633.
22. Sicari, B.M., Rubin, J.P., Dearth, C.L., Wolf, M.T., Ambrosio, F., Boninger, M., Turner, N.J., Weber, D.J., Simpson, T.W., Wyse, A., et al. (2014). An acellular biologic scaffold promotes skeletal muscle formation in mice and humans with volumetric muscle loss. Sci. Transl. Med. *6*, 234ra58–234ra258.
23. Brown, A.L., Brook-Allred, T.T., Waddell, J.E., White, J., Werkmeister, J.A., Ramshaw, J.A.M., Bagli, D.J., and Woodhouse, K.A. (2005). Bladder acellular matrix as a substrate for studying *in vitro* bladder smooth muscle–urothelial cell interactions. Biomaterials *26*, 529–543.
24. Reddy, P.P., Barrieras, D.J., Wilson, G., Bägli, D.J., McLORIE, G.A., Khoury, A.E., and Merguerian, P.A. (2000). Regeneration of functional bladder substitutes using large segment acellular matrix allografts in a porcine model. J. Urol. *164*, 936–941.
25. Brown, B.N., and Badylak, S.F. (2014). Extracellular matrix as an inductive scaffold for functional tissue reconstruction. Transl. Res. *163*, 268–285.
26. Badylak, S.F., and Gilbert, T.W. (2008). Immune Response to Biologic Scaffold Materials, *2* (Elsevier), pp. 109–116.
27. Brown, B.N., Valentin, J.E., Stewart-Akers, A.M., McCabe, G.P., and Badylak, S.F. (2009). Macrophage phenotype and remodeling outcomes in response to biologic scaffolds with and without a cellular component. Biomaterials *30*, 1482–1491.
28. Brown, B.N., Londono, R., Tottey, S., Zhang, L., Kukla, K.A., Wolf, M.T., Daly, K.A., Reing, J.E., and Badylak, S.F. (2012). Macrophage phenotype as a predictor of constructive remodeling following the implantation of biologically derived surgical mesh materials. Acta Biomater. *8*, 978–987.
29. Allman, A.J., McPherson, T.B., Merrill, L.C., Badylak, S.F., and Metzger, D.W. (2002). The Th2-restricted immune response to xenogeneic small intestinal submucosa does not influence systemic protective immunity to viral and bacterial pathogens. Tissue Eng. *8*, 53–62.
30. Wang, X., Chung, L., Hooks, J., Maestas, D.R., Lebid, A., Andorko, J.I., Huleihel, L., Chin, A.F., Wolf, M., Remlinger, N.T., et al. (2021). Type 2 immunity induced by bladder extracellular matrix enhances corneal wound healing. Sci. Adv. *7*, eabe2635.
31. Surucu, Y., Bengur, F.B., Yang, K.S., Schilling, B.K., Baker, J.S., Shabbir, S., Fisher, R., Epperly, M.W., Greenberger, J.S., Rubin, J.P., and Ejaz, A. (2022). Establishment of a Robust and Reproducible Model of Radiation-Induced Skin and Muscle Fibrosis. JoVE, e64251. https://doi.org/10.3791/64251.
32. Inserra, M.M., Bloch, D.A., and Terris, D.J. (1998). Functional indices for sciatic, peroneal, and posterior tibial nerve lesions in the mouse. Microsurgery *18*, 119–124.
33. Huleihel, L., Dziki, J.L., Bartolacci, J.G., Rausch, T., Scarritt, M.E., Cramer, M.C., Vorobyov, T., LoPresti, S.T., Swineheart, I.T., and White, L.J. (2017). Macrophage Phenotype in Response to ECM Bioscaffolds (Elsevier), pp. 2–13.
34. Slivka, P.F., Dearth, C.L., Keane, T.J., Meng, F.W., Medberry, C.J., Riggio, R.T., Reing, J.E., and Badylak, S.F. (2014). Fractionation of an ECM hydrogel into structural and soluble components reveals distinctive roles in regulating macrophage behavior. Biomater. Sci. *2*, 1521–1534.
35. Kokai, L.E., Schilling, B.K., Chnari, E., Huang, Y.-C., Imming, E.A., Karunamurthy, A., Khouri, R.K., D'Amico, R.A., Coleman, S.R., Marra, K.G., and Rubin, J.P. (2019). Injectable allograft adipose matrix supports adipogenic tissue remodeling in the nude mouse and human. Plast. Reconstr. Surg. *143*, 299–309e.
36. Ejaz, A., Yang, K.S., Venkatesh, K.P., Chinnapaka, S., Kokai, L.E., and Rubin, J.P. (2020). The impact of human lipoaspirate and adipose tissue-derived stem cells contact culture on breast cancer cells: Implications in breast reconstruction. Int. J. Mol. Sci. *21*, 9171.
37. Khonji, N. (2010). Breast reconstruction using autologous fat. Br. J. Surg. *97*, 795–796. https://doi.org/10.1002/bjs.7101.
38. Kølle, S.F.T., Fischer-Nielsen, A., Mathiasen, A.B., Elberg, J.J., Oliveri, R.S., Glovinski, P.V., Kastrup, J., Kirchhoff, M., Rasmussen, B.S., Talman, M.L.M., et al. (2013). Enrichment of autologous fat grafts with ex-vivo expanded adipose tissue-derived stem cells for graft survival: a randomised placebo-controlled trial. Lancet *382*, 1113–1120. https://doi.org/10.1016/S0140-6736(13)61410-5.
39. Rigotti, G., Marchi, A., Galiè, M., Baroni, G., Benati, D., Krampera, M., Pasini, A., and Sbarbati, A. (2007). Clinical treatment of radiotherapy tissue damage by lipoaspirate transplant: a healing process mediated by adipose-derived adult stem cells. Plast. Reconstr. Surg. *119*, 1409–1422.
40. Akita, S., Yoshimoto, H., Ohtsuru, A., Hirano, A., and Yamashita, S. (2012). Autologous adipose-derived regenerative cells are effective for chronic intractable radiation injuries. Radiat. Prot. Dosimetry *151*, 656–660. https://doi.org/10.1093/rpd/ncs176.
41. Mizuno, H., and Hyakusoku, H. (2010). Fat grafting to the breast and adipose-derived stem cells: recent scientific consensus and controversy. Aesthet. Surg. J. *30*, 381–387. https://doi.org/10.1177/1090820X10373063.
42. Faghahati, S., Delaporte, T., Toussoun, G., Gleizal, A., Morel, F., and Delay, E. (2010). [Treatment by fat tissue transfer for radiation injury in childhood facial cancer]. Ann. Chir. Plast. Esthet. *55*, 169–178. https://doi.org/10.1016/j.anplas.2009.05.004.
43. Ejaz, A., Epperly, M.W., Hou, W., Greenberger, J.S., and Rubin, J.P. (2019). Adipose-derived stem cell therapy ameliorates ionizing irradiation fibrosis via hepatocyte growth factor-mediated transforming growth factor-β downregulation and recruitment of bone marrow cells. Stem Cell. *37*, 791–802.
44. Adem, S., Abbas, D.B., Lavin, C.V., Fahy, E.J., Griffin, M., Diaz Deleon, N.M., Borrelli, M.R., Mascharak, S., Shen, A.H., Patel, R.A., et al. (2022). Decellularized adipose matrices can alleviate radiation-induced skin fibrosis. Adv. Wound Care *11*, 524–536.
45. Dong, X.R., and Majesky, M.W. (2012). Restoring Elastin with microRNA-29. Am. Heart Assoc.
46. Ejaz, A., Greenberger, J.S., and Rubin, P.J. (2019). Understanding the mechanism of radiation induced fibrosis and therapy options. Pharmacol. Ther. *204*, 107399.
47. Borovikova, A.A., Ziegler, M.E., Banyard, D.A., Wirth, G.A., Paydar, K.Z., Evans, G.R.D., and Widgerow, A.D. (2018). Adipose-Derived

Tissue in the Treatment of Dermal Fibrosis: Antifibrotic Effects of Adipose-Derived Stem Cells. Ann. Plast. Surg. *80*, 297–307.

48. Rosu-Myles, M., Stewart, E., Trowbridge, J., Ito, C.Y., Zandstra, P., and Bhatia, M. (2005). A unique population of bone marrow cells migrates to skeletal muscle via hepatocyte growth factor/c-met axis. J. Cell Sci. *118*, 4343–4352.
49. Xin, X., Yang, S., Ingle, G., Zlot, C., Rangell, L., Kowalski, J., Schwall, R., Ferrara, N., and Gerritsen, M.E. (2001). Hepatocyte growth factor enhances vascular endothelial growth factor-induced angiogenesis *in vitro* and *in vivo*. Am. J. Pathol. *158*, 1111–1120.
50. Giannopoulou, M., Dai, C., Tan, X., Wen, X., Michalopoulos, G.K., and Liu, Y. (2008). Hepatocyte growth factor exerts its anti-inflammatory action by disrupting nuclear factor-κB signaling. Am. J. Pathol. *173*, 30–41.
51. Liu, Y. (2004). Hepatocyte growth factor in kidney fibrosis: therapeutic potential and mechanisms of action. Am. J. Physiol. Renal Physiol. *287*, F7–F16.
52. Braga, T.T., Agudelo, J.S.H., and Camara, N.O.S. (2015). Macrophages During the Fibrotic Process: M2 as Friend and Foe. Front. Immunol. *6*, 602. https://doi.org/10.3389/fimmu.2015.00602.
53. Dainiak, N., Gent, R.N., Carr, Z., Schneider, R., Bader, J., Buglova, E., Chao, N., Coleman, C.N., Ganser, A., Gorin, C., et al. (2011). Literature review and global consensus on management of acute radiation syndrome affecting nonhematopoietic organ systems. Disaster Med. Public Health Prep. *5*, 183–201.
54. Evangelista-Leite, D., Carreira, A.C.O., Gilpin, S.E., and Miglino, M.A. (2022). Protective Effects of Extracellular Matrix-Derived Hydrogels in Idiopathic Pulmonary Fibrosis. Tissue Eng. Part B Rev. *28*, 517–530.
55. Nepon, H., Safran, T., Reece, E.M., Murphy, A.M., Vorstenbosch, J., and Davison, P.G. (2021). Radiation-induced Tissue Damage: Clinical Consequences and Current Treatment Options, *3* (Thieme Medical Publishers, Inc.), pp. 181–188.
56. Kang, E., Han, S., Lee, W., Kim, S., and Yang, C. (2022). Effects of the Acellular Dermal Matrix and Fat Graft on Radiation-Induced Fibrosis in a Prosthesis-Implanted Rat Model. World J. Surg. Surgical Res. *5*, 1387.
57. Brand, R.M., Epperly, M.W., Stottlemyer, J.M., Skoda, E.M., Gao, X., Li, S., Huq, S., Wipf, P., Kagan, V.E., Greenberger, J.S., and Falo, L.D., Jr. (2017). A topical mitochondria-targeted redox-cycling nitroxide mitigates oxidative stress-induced skin damage. J. Invest. Dermatol. *137*, 576–586.
58. Kalash, R., Epperly, M.W., Goff, J., Dixon, T., Sprachman, M.M., Zhang, X., Shields, D., Cao, S., Franicola, D., Wipf, P., et al. (2013). Amelioration of radiation-induced pulmonary fibrosis by a water-soluble bifunctional sulfoxide radiation mitigator (MMS350). Radiat. Res. *180*, 474–490.
59. Steinman, J., Epperly, M., Hou, W., Willis, J., Wang, H., Fisher, R., Liu, B., Bahar, I., McCaw, T., Kagan, V., et al. (2018). Improved Total-Body Irradiation Survival by Delivery of Two Radiation Mitigators that Target Distinct Cell Death Pathways. Radiat. Res. *189*, 68–83. https://doi.org/10.1667/RR14787.1.
60. Hamade, D.F., Epperly, M.W., Fisher, R., Hou, W., Shields, D., van Pijkeren, J.-P., Mukherjee, A., Yu, J., Leibowitz, B.J., Vlad, A.M., et al. (2023). Release of Interferon-β (IFN-β) from Probiotic Limosilactobacillus reuteri-IFN-β (LR-IFN-β) Mitigates Gastrointestinal Acute Radiation Syndrome (GI-ARS) following Whole Abdominal Irradiation. Cancers *15*, 1670.
61. Chinnapaka, S., Yang, K.S., Samadi, Y., Epperly, M.W., Hou, W., Greenberger, J.S., Ejaz, A., and Rubin, J.P. (2021). Allogeneic adipose-derived stem cells mitigate acute radiation syndrome by the rescue of damaged bone marrow cells from apoptosis. Stem Cells Transl. Med. *10*, 1095–1114.

STAR★METHODS

KEY RESOURCES TABLE

REAGENT or RESOURCE	SOURCE	IDENTIFIER
Antibodies		
Rabbit Collagen III	Proteintech	Cat # 22734-1-AP
Rabbit Elastin	abcam	Cat # ab307150
Rabbit Collagen I	Novus Biologicals	Cat # NB600-408
Biological samples		
Mouse adipose tissue	This paper	N/A
Mouse adipose derived stem cells	This paper	N/A
Endothelial cells HUVEC	ATCC	N/A
Mouse fibroblasts L929	ATCC	N/A
Chemicals, peptides, and recombinant proteins		
Human adipose derived extracellular matrix	MTF Biologics	Renuva
Critical commercial assays		
Mouse Luminex Assay	R&D SYSTEMS	N/A
Experimental models: Cell lines		
Endothelial cells HUVEC	ATCC	N/A
Mouse fibroblasts L929	ATCC	N/A
Oligonucleotides		
KiCqStart SYBR Green primers	Millipore Sigma	N/A
Software and algorithms		
GraphPad Prism	GraphPad by Dotmatics	N/A
ImageJ	NIH	N/A

RESOURCE AVAILABILITY

Lead contact

Further information and requests for resources and reagents should be directed to and will be fulfilled by the lead contact, Asim Ejaz (ejaza@upmc.edu).

Materials availability

This study did not generate new unique reagents.

Data and code availability

- All data reported in this paper is available from the lead contact upon request.
- This paper does not report original code.
- Any additional information required to reanylyze the data reported in this paper is available from the lead contact upon request.

EXPERIMENTAL MODEL AND STUDY PARTICIPANT DETAILS

All C57BL/6, C57BL/6 GFP^{+}/Luc$^{+,}$ and C57BL/6 HGF$^{fl/fl}$ mice were housed in an Association for Assessment and Accreditation of Laboratory Animal Care International (AAALAC)-approved facility and were treated according to the National Institutes of Health Guide for the Care and Use of Laboratory Animals. All experiments were approved by the University of Pittsburgh IACUC committee. Irradiation of mice was carried out as explained.[31] Mice's legs were shaved 2-3 days before irradiation. Mice were anesthetized by 1.25 mg/kg of Nembutal (Lundbeck, Copenhagen, Denmark) intraperitoneal injection. Mice were positioned in the radiation field and secured by tape to achieve targeted irradiation.

A 6-MeV electron beam from a Varian 23EX linear accelerator (Varian Medical Systems, Inc., Palo Alto, CA) was used to generate β-irradiation burns. Irradiation was conducted using a 25 × 25 cm applicator, a source-to-skin distance of 100 cm, and a dosage rate of 1,000 MU/minute. During irradiation, a 1-cm–thick bolus was placed to prevent the deep penetration of radiations. The setup is such that only the shaved upper right rear leg of each mouse was exposed to an irradiation field of 25 × 25 cm. All monitor units were calculated by incorporating the appropriate applicator factor and cutout factors such that the dose delivered to mouse skin was 40 Gy.

METHOD DETAILS

Adipose-derived extracellular matrix

Adipose-derived extracellular matrix (Ad-ECM) was procured from MTF Biologics (NJ, USA) in a paste form under the trade name Renuva®. A subcutaneous pocket was created with a standard escharotomy with a 16 gauge needle, and a single dose of 200 μl was injected subcutaneously at the irradiated site.

Leg contracture measurements

The extent of the leg movement was measured using a protractor and represented as the degree of motion.[31] Mice were anesthesized using isoflurane. Fix the protractor with tape on the bench adjacent nose cone supplying isoflurane. Position the right knee to the protractor's center and keeping the knee fixed using the left hand and use the right hand to dorsiflex the foot with the index and pollex fingers. Note the degree of extension by reading the value indicated by toes.

Measurement of gait functional index

The gait functional index was measured as published earlier.[31] A 3D-printed rodent walking track was used to create a 40 cm walking path at a suspension height of 15 cm. Mice gait was recorded using a camera and still frames were analyzed using Image J. Foot length, outer toe spread and inner toe spread were measured and gait index was calculated.

Histological evaluation of skin damage and collagen deposition

Tissue samples were fixed in 10% formalin, embedded in paraffin, and cut into 5-μm sections. Relative collagen levels were assessed using Masson's trichrome staining. Slides were examined by a pathologist for signs of fibrosis. Skin sections were evaluated for signs of skin damage via hematoxylin and eosin stains.[31,57] Masson's Trichrome stained skin sections were scored blindly for inflammation, fibrosis, vascularity, and cellular alteration following the published guidelines.[6]

Immunofluorescence staining

Paraffin skin sections were stained with collagen 1, collagen 3, and Elastin antibodies (Protein Tech, USA) followed by staining with fluorescent-labeled secondary antibodies. DAPI (Sigma, USA) was employed as a nuclear stain. Stained sections were imaged using a fluorescent microscope (Keyence, Japan).

Isolation of adipose-derived stem cells

Subcutaneous adipose tissue from mice was harvested under sterile conditions. The tissue was cut into pieces (∼ 1–2 mg) and digested in digestion buffer (HBSS (Fisher Scientific, MA, USA) containing 200 U/ml collagenases (CLS Type I, Worthington Biochemical Corp., Lakewood, NJ) and 2% w/v BSA (Sigma, USA) under stirring for 60 min at 37°C and 450 rpm; 1 mg adipose tissue/3 ml digestion buffer. The dispersed tissue was centrifuged for 5 min at 200 RCF at room temperature. The floating adipocytes were aspirated, and the sedimented stromal-vascular fraction (SVF) was suspended in erythrocyte lysis buffer (Fisher Scientific, MA, USA) and incubated for 2 min at room temperature. To remove tissue debris the cell suspension was filtered through a nylon mesh (pore size 100 μm, BD, USA). After another centrifugation step (5 min at 200 RCF) the pelleted SVF was suspended in DMEM (Fisher Scientific, MA, USA) 10% FBS (Sigma), and filtered through a 70 μm mesh to remove residual cell aggregates. SVF cells were inoculated at a density of 30,000/cm^2. The attached cell population was referred to as the adipose-derived stromal cell (ASC) fraction which was used for further studies. Cells in passages 4-5 are used in this study.

Chimeric mice generation

Chimeric mice were generated as published.[18] C57BL/6 mouse - GFP^+ Luc^+ marrow chimeric mice were prepared with 10 Gy total-body irradiation; followed by i.v injection of 1 × 10^6 GFP^+ Luc^+ marrow cells 24 h later.[58] Chimerism was documented by bioluminescence imaging as reported.[58]

Transwell co-culture

A Transwell system (0.4 μm pore size, Polyester (PET) membrane; Corning, USA) was employed. Mouse adipose-derived stem cells or mouse bone marrow cells were cultured in the top transwell basket compartment, while mouse fibroblast or Ad-ECM was cultured in the lower compartment. A schematic of the co-culture approach is shown in Figure 5C. For studying the role of HGF in fibrosis mitigation, mouse fibroblasts were grown to confluence and irradiated using a 10Gy radiation dose. Twenty-four hours post-irradiation 3 ×10^5 ASCs were added to

the upper transwell basket. Co-culture was maintained for 48 hours. Cells were lysed, and total RNA was isolated using TRIzol (Sigma, USA) reagent following the manufacturer's protocol. cDNA was synthesized and expression of pro-fibrotic gene battery (TGF β1, CTGF, NF-κB, IL-1, Collagens 1-6) was analyzed using gene-specific primers employing quantitative real-time PCR.

Real-time PCR

RNA was extracted from mouse skin or cultured cells using the TRIzol reagent following the manufacturer's instructions. RNA was reverse transcribed using a High Capacity cDNA Reverse Transcription Kit (Applied Biosystems, USA) according to the manufacturer's protocol. Using cDNA as a template and gene-specific primers (MilliporeSigma, USA) expression of IL-1, IL-2, IL-6, TGF β1, TNF, NF-κB, and Collagens 1-6 was quantified by quantitative real-time PCR using the Eppendorf Realplex2 Mastercycler. Data for each gene transcript were normalized by calculating the difference (ΔCt) from the Ct-housekeeping and Ct-Target genes. The relative increase or decrease in expression was calculated by comparing the reference gene with the target gene calculated by comparing the reference gene with the target gene (ΔΔCt) and using the formula for relative expression ($=^{2\Delta\Delta Ct}$).

Luminex assay

Concentrations of GM-CSF, G-CSF, M-CSF, VEGFA, TNFα, IL-1β, IL-6, IL-17, CXCL-1, Eotaxin, CXCL5, CXCL10, CCL-2, CCL-3, CCL-4, TGFβ, MIG-2, IL-4, IL-5, IL-15 were analyzed employing a multiplex mouse Luminex™ assay from R&D Systems according to manufacturer protocol.[59] Fresh frozen skin tissue were processed as explained.[60] Samples were diluted 2-fold by adding 75μl supernatant to 75 μl of Calibrator Diluent mix (Kit). Add 50 μl sample or standard (Kit) to 96 well plates according to the assay scheme. Incubate for 2 hours at room temperature after adding 50 μl Microparticle Cocktail (Kit). Wash 3 times with 100 μl wash buffer (Kit). Add 50 μl diluted biotin antibody cocktail to each well and incubate for 1 hour with shaking at 800 rpm. Wash 3 times with wash buffer. Add 50 μl diluted Streptavidin-PE to each well and incubate for 30 minutes with shaking at 800 rpm. Wash again 3 times with wash buffer. Readings were taken using Luminex 100/200™ analyzer (Luminex Inc., Austin, TX.), and protein concentrations were reported.[61]

Digestion of Ad-ECM

Ad-ECM (10mg/ml) was incubated with pepsin (1mg/ml) in 0.01M HCl (pH 2.0) for 48 hours at room temperature under continuous stirring.[34] The slurry was neutralized to a pH of 7.4 in PBS centrifuged at 20,000g for 2 hours and supernatant collected having protein concentration 1.8 mg/ml that is used for downstream cell treatment studies following sterile filtration and quantification. We observed no gelation of digested Ad-ECM.

QUANTIFICATION AND STATISTICAL ANALYSIS

All data is reported as the mean ± standard deviation to assess the between-subject variability of the measured outcome. Student's T-test and Analysis of variance (ANOVA) test was performed where applicable using GraphPad Prism software.